Cement and Concrete Research 74 (2015) 116–125

Contents lists available at ScienceDirect

Cement and Concrete Research

journal homepage: http://ees.elsevier.com/CEMCON/default.asp

Influence of silica fume on the microstructure of cement pastes: New insights from ^{1}H NMR relaxometry

A.C.A. Muller [a,*], K.L. Scrivener [a], J. Skibsted [b], A.M. Gajewicz [c], P.J. McDonald [c]

[a] Laboratory of Construction Materials, Ecole Polytechnique Fédérale de Lausanne, CH-1015 Lausanne, Switzerland
[b] Department of Chemistry and Interdisciplinary Nanoscience Center (iNANO), Aarhus University, DK-8000 Aarhus C, Denmark
[c] Department of Physics, University of Surrey, Guildford, Surrey GU2 7XH, UK

ARTICLE INFO

Article history:
Received 2 July 2014
Accepted 20 April 2015
Available online 16 May 2015

Keywords:
^{1}H NMR (B)
Silica fume (D)
C–S–H composition (B)
Density (B)

ABSTRACT

^{1}H NMR has been used to characterise white Portland cement paste incorporating 10 wt.% of silica fume. Samples were measured sealed throughout the hydration without sample drying. Paste compositions and C–S–H characteristics are calculated based on ^{1}H NMR signal intensities and relaxation analysis. The results are compared with a similar study of plain white cement paste. While the presence of silica fume has little influence on C–S–H densities, the chemical composition is impacted. After 28 days of sealed hydration, the Ca/(Si + Al) ratio of the C–S–H is 1.33 and the H_2O/(Si + Al) ratio is 1.10 when 10% of silica fume is added to the white cement. A densification of the C–S–H with time is observed. There are no major changes in capillary, C–S–H gel and interlayer pore sizes for the paste containing silica fume compared to the plain white cement paste. However, the gel/interlayer water ratio increases in the silica fume blend.

1. Introduction

Basic cement hydration involves the dissolution of alite (C_3S) and belite (C_2S) with the formation, by precipitation, of calcium silicate hydrates (C–S–H) and calcium hydroxide (CH, also called "portlandite"). While calcium hydroxide is a very well known crystalline phase [1,2], the C–S–H structure, chemical composition, density and morphology remain uncertain [3]. The primary reasons are twofold: first, C–S–H is a highly disordered nanoscale material incorporating a significant amount of water that is difficult to probe experimentally. Only a few techniques are able to adequately characterise as-prepared C–S–H without removing the water, a procedure that damages the nanoscale structures that are of interest. Secondly, the way C–S–H precipitates is highly dependent on the chemical and physical conditions in which the hydration takes place [4–6]. The different phenomena leading to C–S–H precipitation become even more complex when supplementary cementitious materials (SCMs) are used. Some SCMs act only as nucleation sites for the C–S–H to grow: the so-called filler effect [7]; others cause pozzolanic reactions, i.e., the consumption of CH to form more C–S–H.

Silica fume is a by-product from the production of elemental silicon and its alloys. Silica fume is typically used at replacement levels of 5–10% in high performance concrete to improve strength and durability. It not only can react with calcium hydroxide to produce C–S–H, but also modifies the microstructure of the cement paste due to its fine particle size. Many studies describe changes due to addition of silica fume. Skibsted et al. [8] used the ^{29}Si MAS NMR technique to quantify the reaction degree of 10% of silica fume in white cement pastes at water-to-cement ratio, $w/c = 0.5$. They found 65% of silica fume reaction by 100 days. Justnes et al. [9] investigated the hydration of C_3S and C_2S with condensed silica fume. Mixes with silica fume had an increased C–S–H mean chain length compared to mixes without silica fume. Justnes et al. [10] also found an acceleration of the cement reaction at early age in the presence of silica fume and estimated a lower Ca/Si of the C–S–H in mixes with silica fume knowing additionally the non-evaporable water content measured by TGA. However, despite these studies, there is no description of the changes affecting the nanostructure of C–S–H and its evolution with time in never dried systems. Moreover, the C–S–H density has not been reported for Portland cement with silica fume addition.

^{1}H NMR relaxometry has been used sporadically to study cement pastes over several decades. A recent paper from Valori et al. [11] reviews the progress made in characterising cement-based materials by water relaxation techniques and states the current knowledge of applying ^{1}H NMR to cement. We have shown in recent publications [12,13] how quantitative non-invasive ^{1}H NMR relaxometry can be used to fully describe plain white Portland cement pastes including pore sizes, C–S–H chemical composition and the evolution of C–S–H density over time. The Powers and Brownyard's diagram [14] was revised based on ^{1}H NMR signal intensities and relation analysis. In this work, we use ^{1}H NMR relaxation analysis techniques to identify

* Corresponding author. Tel.: 41 77 479 80 47.
E-mail address: arnaudc.muller@epfl.ch (A.C.A. Muller).

http://dx.doi.org/10.1016/j.cemconres.2015.04.005

the changes of material properties due to the incorporation of 10% silica fume as a replacement of cement mass. The objective is to investigate the impact of this SCM on the C–S–H characteristics and more generally on the pore network of the cement paste. We show the evolution of the different water populations as the hydration progresses, linked in parallel with calculated C–S–H density, C–S–H chemical composition and silica fume reaction.

2. Methods

White Portland cement was used in this study to minimise excess paramagnetic species (e.g., Fe^{3+} ions) that can enhance relaxation. It was composed of C_3S ($f_{C3S} = 67$ wt.%), C_2S ($f_{C2S} = 20\%$), C_3A ($f_{C3A} = 3.6\%$) and sulphate phases ($f_{sp} = 4.7\%$) with all other phases representing less than 1% of the mass. The cement has a Fe_2O_3 content of 0.34 wt.%, a density of 3.15 g/cm^3 and a specific surface area of $\approx$0.2 m^2/g. Condensed silica fume was provided by Elkem under the name "Microsilica 983 U"; it is made of 98.6% amorphous silica, has an absolute density of 2.27 g/cm^3 and a specific surface area of $\approx$20 m^2/g.

Pastes with 10% cement mass replacement by silica fume were made according to the following procedure. The silica fume was first pre-dispersed in distilled water for 8 min at 15,000 rpm in an ultrasonic bath. No superplasticizer was used for rheological or dispersive purposes in order not to introduce hydrogen atoms other than those in water which might affect the ^{1}H NMR experiments. Then the water with suspended silica fume was added to the cement to achieve a water-to-binder ratio of $w/b = 0.4$ by weight. All components were mixed together for 5 min at 1600 rpm with a paste mixer LABORTECHNIK RW 20.n. Small amounts of paste ($\approx$ 0.35 cm^3) were deposited at the bottom of glass ^{1}H NMR tubes and sealed with parafilm®. Multiple samples cast at different times were intermittently measured in a temperature-controlled ^{1}H NMR probe. Other samples were cast in larger containers and parallel experiments were carried out throughout hydration using X-ray diffraction with Rietveld analysis (XRD), isothermal calorimetry, solid-state ^{29}Si MAS NMR, scanning electron microscopy with energy dispersive X-ray (SEM–EDX), transmission electron microscopy (TEM) and thermo-gravimetric analysis (TGA). As a reference material we use a plain white cement paste with $w/c = 0.4$, described and characterised in reference [12]. All samples were measured and cured under sealed conditions at 20 °C.

^{1}H NMR measurements were made on a Bruker Minispec NMR spectrometer operating at 7.5 MHz. Both quadrature (solid) echo [15] and Carr–Purcell–Meiboom–Gill CPMG [16] (spin) echo measurements were carried out. ^{1}H NMR experimental parameters are as in Ref. [12]. The quadrature echo signals were deconvoluted into a Gaussian and an exponential decay part. The exponential fraction arises from the mobile water within the sample and is not pulse gap dependent. The Gaussian intensity decay is assigned to water in solid crystalline phases [12,13]. The amplitude of this component depends on the pulse gap. Pulse gaps were varied in the range 15–45 μs and the amplitude was back extrapolated to zero pulse gap free from relaxation phenomena using Gaussian fitting. The mobile part of the signal was separately resolved into different T_2 components using the CPMG pulse sequence as in [12]. For this, the inverse Laplace transform (ILT) algorithm developed by Venkataramanan et al. [17] was applied to the CPMG echo intensity decay. More details about measurements and analysis of ^{1}H NMR relaxation characteristics are given in [12].

XRD measurements of as-prepared sealed pastes were first performed on slices right after cutting. Hydration of other samples was stopped by immersion in isopropanol for 7 days. Such samples were then vacuum dried, crushed and measured as a powder. A Panalatical X'Pert Pro MPD diffractometer in a θ–θ configuration was used with a CuKα source (wavelength 1.54 Å) and a fixed divergence slit of 0.5°. Samples were scanned on a rotating stage between 7 and 70° (2θ) using a X'Celerator detector with a step size of 0.0167° (2θ) and a time step of 77.5 s.

The chemical shrinkage was recorded by the conventional technique of following the water height in a pipette above hydrating paste. Chemical shrinkage measurements require samples to be exposed to excess water. Therefore, the hydration is different from samples sealed cured. The degrees of hydration for underwater pastes were also measured by XRD.

The heat released from sealed hydrating pastes was recorded with an isothermal calorimeter (TAM Air from TA Instruments). It consists of 8 parallel twin measurement channels maintained at a constant temperature: one for the paste sample (approximately 10 g), the other for the reference sample. The instrument was maintained in a temperature-controlled room to ensure the stability of the baseline. Measurements were carried out for 28 days at 20 °C.

The solid-state ^{29}Si MAS NMR spectra were recorded at a magnetic field of 9.4 T on a Varian Unity INOVA-400 spectrometer, using a home-built CP/MAS probe for 7 mm o.d. rotors with sample volumes of 220 μL. The single-pulse experiments employed a spinning speed of $\nu_R = 6.0$ kHz, a 45° excitation pulse ($\tau_{pw} = 3.0$ μs) and a repetition delay of 60 s. Typically 1024–2048 scans were recorded for each spectrum. The ^{29}Si chemical shifts in the ^{29}Si MAS NMR spectra are reported in parts per million relative to an external sample of neat tetramethylsilane (TMS), using an external sample of β-Ca_2SiO_4 ($\delta_{iso} = -71.33$ ppm) as a secondary reference material.

For the microscopy, a FEI Quanta 200 SEM equipped with a tungsten filament was used. It was operated at 15 kV with a spot size small enough to have a sufficient BSE image resolution (to allow the user to reasonably position the EDS points) and a relatively low beam current (0.7–0.8 nA), but high enough to achieve 12–15 kilocounts per second in hydrated phases. The detector is a Bruker AXS XFlash® Detector 4030 (with an active surface of 30 mm^2) with a take-off angle of 35°, i.e., an optimal working distance of 12.5 mm.

The TEM is a FEI Technai Osiris™ (CIME, EPFL). It was operated at 80 kV and adjusted to yield a low beam current in order to minimise damage. Imaging and EDS were done in STEM mode. Quantification of the spectra was done using a standardless Cliff–Lorimer method with a thickness chosen at 150 nm as a reasonable average, and assuming an average density of 2.6 g/cm^3 for the C–S–H layers.

TGA measurements were made on dried powders, after being 7 days in isopropanol and 7 days in a desiccator, with a Mettler Toledo TGA/SDTA 851 analyser operating between 30 and 950 °C at 10 °C/min under N_2 gas flow to prevent carbonation.

3. ^{1}H NMR analysis

^{1}H NMR probes the water, or more precisely the hydrogen protons, within filled pores and solid phases. It has been shown that the NMR signal quantitatively reveals all the water in the sample [13,18]. In the so-called fast diffusion limit, the signal lifetime of water in pores, known as the spin–spin relaxation time T_2, is very sensitive to pore size with $\frac{1}{T_2} \propto \frac{\lambda S}{V}$ where λ is the surface relaxivity, S is the surface area and V is the volume of the pore [19–21]. T_2 of water in pores of cement pastes varies from 100 μs to 100 ms [12,13]. The T_2 of water bound in solid phases is even shorter, circa 10 μs [18]. By combining solid echo and CPMG pulse sequences, the NMR technique is able to see and quantify all hydrogen protons within the cement paste [12,13]. Four water locations can be identified: the chemically combined water within the crystalline phases portlandite and ettringite (with NMR signal fraction called I_{solid}); C–S–H interlayer water (I_{CSH}); water in C–S–H gel pores (I_{gel}); and water in larger capillary pores becoming interhydrate spaces (I_{cap}). The different I-values represent the measured NMR signal fraction as $I_{solid} + I_{CSH} + I_{gel} + I_{cap} = 1$. The linear behaviour of the NMR signal intensity as a function of mass loss during progressive drying of the sample [13] and the very good agreement between the I_{solid} NMR signal and the water in crystalline phases as measured by XRD/TGA [12] give us confidence that we properly account for all hydrogen protons within the paste. Hydrogen signal arises entirely from mixing water i.e., the initial

0.4 g of water per gramme of binder. Since the paste is kept sealed, empty volumes are created by chemical shrinkage during hydration which are not measured by the NMR experiment.

Mass and volume balance equations for the paste in terms of NMR signal intensities were previously written [12]. For this work, the calculations are modified to incorporate the contribution of 10% of silica fume. The revised equations for 1 g of binder (cement + silica fume) are written as:

$$1+\frac{w}{b}=0.9(1-\alpha_c)+0.1(1-\alpha_{sf})+\frac{w}{b}\left[\beta I_{solid}+\gamma I_{CSH}+\delta\left(I_{gel}+I_{cap}\right)\right] \quad (1)$$

$$\frac{0.9}{\rho_c}+\frac{0.1}{\rho_{sf}}+\frac{w}{b\rho_w}=\frac{0.9(1-\alpha_c)}{\rho_c}+\frac{0.1(1-\alpha_{sf})}{\rho_{sf}}+\frac{w}{b}\left[\frac{\beta I_{solid}}{\rho_{solid}}+\frac{\gamma I_{CSH}}{\rho_{CSH}}+\frac{\delta\left(I_{gel}+I_{cap}+I_{void}\right)}{\rho_w}\right]. \quad (2)$$

The left hand side of Eq. (1) (mass) and Eq. (2) (volume) corresponds to the state of the paste at time of mixing. The right hand side represents the sum of the different components of the paste at any subsequent hydration time. The hydration products formed are expressed by their respective water mass written in terms of NMR signals. w/b represents the initial water-to-binder ratio of the paste and remains constant over time due to the sealing of the sample. α stands for degree of hydration. The subscripts w, b, c, sf and $void$ refer to water, binder, cement, silica fume and chemical shrinkage respectively; the others are clear from the text. The parameters β, γ and δ are the inverse water mass fractions in crystalline phases, C–S–H and pore fluid, respectively. The solid water signal, I_{solid}, can be decomposed into $I_{solid}=I_{CH}+I_{ett}$, where CH means portlandite and ett ettringite. I_{ett} can be measured by XRD, allowing the deconvolution of the I_{solid} signal. Inverse water contents of portlandite and ettringite are $\beta_{CH}=74/18$ and $\beta_{ett}=1255/576$. The mass of crystalline phases in the sample, per gramme of binder, is then decomposed as $(w/b)\beta I_{solid}=(w/b)(\beta_{CH}I_{CH}+\beta_{ett}I_{ett})$. We treat the pore fluid as water, so that $\delta=1$. The Eq. (2) reworks Eq. (1) by dividing product masses by their respective densities, ρ. Crystalline phase densities are taken from literature as $\rho_{CH}=2.24$ g/cm^3 and $\rho_{ett}=1.77$ g/cm^3. ρ_w is assumed to be 1 g/cm^3.

The chemical shrinkage volume, not seen by NMR, is required. The chemical shrinkage volume, normalised per gramme of binder, is expressed as an equivalent water signal fraction (I_{void}). It takes the total NMR signal intensity above unity. At any given time, $I_{void}=V_{void}/(w/b)$, where V_{void} is the chemical shrinkage volume, or voidage, in cm^3 per gramme of binder.

For density calculation, the degrees of reaction of cement and silica fume are required. For cement, careful XRD Rietveld quantifications were done sufficiently frequently to capture the consumption kinetics of C_3S and C_2S. In parallel, ^{29}Si MAS NMR quantifies the degree of reaction of the 10% of silica fume incorporated initially into the mix. Isothermal calorimetry is used to confirm the trends.

In our calculation, further equations are required to calculate the chemical composition of the C–S–H, expressed as $Ca_z(Si_y,Al_{(1-y)})O_{(z+1/2y+3/2)}(H_2O)_x$. The Ca/(Si + Al) ratio can be balanced with:

$$\frac{0.9\left[3\left(\frac{f_{C_3S}\alpha_{C_3S}}{C_3S^{AMU}}\right)+2\left(\frac{f_{C_2S}\alpha_{C_2S}}{C_2S^{AMU}}\right)\right]+1.5\cdot n_{Al}^{CSH}}{0.9\left[\left(\frac{f_{C_3S}\alpha_{C_3S}}{C_3S^{AMU}}\right)+\left(\frac{f_{C_2S}\alpha_{C_2S}}{C_2S^{AMU}}\right)\right]+0.1\left[\frac{\alpha_{sf}}{SiO_2{}^{AMU}}\right]+n_{Al}^{CSH}}=\frac{\frac{I_{CH}n_{Hyd}}{2}+\frac{I_{CSH}n_{Hyd}z}{2x}+1.5\cdot n_{Al}^{CSH}}{\frac{I_{CSH}n_{Hyd}y}{2x}+n_{Al}^{CSH}}$$

where,

$$y=\frac{n_{Si}^{CSH}}{n_{Si}^{CSH}+n_{Al}^{CSH}}=1-\frac{4x\cdot 0.9\left(f_{C3A}-f_{C3A}^{ett}\right)}{I_{CSH}n_{Hyd}C_3A^{AMU}}. \quad (3)$$

Eq. (3) consists of a conservation of the chemical elements Ca, Al and Si in the raw ingredients (cement and silica fume) (left part) and the hydration products (right part). The C_3A that has not been used to precipitate ettringite is assumed to be incorporated in C–S–H. The number of moles of alumina in the C–S–H, n_{Al}^{CSH}, per gramme of binder, can be expressed as $n_{Al}^{CSH}=2\cdot 0.9(f_{C3A}-f_{C3A}^{ett})/C_3A^{AMU}$, where f_{C3A}^{ett} is the C_3A mass fraction in cement which was consumed to form ettringite. The abbreviation AMU denotes atomic mass units and n_{Hyd} represents the number of hydrogen moles per gramme of binder as $n_{Hyd}=2\cdot(w/b)/H_2O^{AMU}$ moles/g of binder.

The inverse water mass fraction of C–S–H, γ, is expressed as a function of calcium (z), silica (y) and water (x) molar contents according to

$$\gamma=\frac{56z+9y+51+18x}{18x} \quad (4)$$

Additionally, the C–S–H can be considered as including gel water with water content (x') in which case

$$x'=x\left(I_{CSH}+I_{gel}\right)/I_{CSH}. \quad (5)$$

More details about the constants and derivations of these equations can be found in our recent publication [12].

4. Results

4.1. Evolution of the different pore water signals

Fig. 1a shows the evolution of the different ^{1}H NMR water signal fractions as a function of hydration time for white cement with 10% silica fume (coloured symbols) and for plain white cement taken from reference [12] (grey symbols + lines), for comparison. The addition of 10% of silica fume in the white cement paste did not cause the appearance of any other population of water, according to ^{1}H NMR relaxometry data, compared to the plain white cement. The I_{solid} signal arises from crystalline phases; two water reservoirs are found within the C–S–H (interlayer and gel water) and the "free water" volume is seen as longer components.

The evolution of the pore populations with hydration of the cement with silica fume is similar to plain white cement. However, there are important differences. The first is that the end of gel pore formation happens after 1 day for the silica fume blend compared to 2 days previously observed for plain white cement paste. The second difference is that the fraction of C–S–H interlayer water (I_{CSH}) is much lower in the presence of silica fume. On the other hand, the fraction of water in C–S–H gel becomes higher and I_{gel} rapidly represents more than 50% of all water within the cement paste. Despite this redistribution between the two C–S–H water populations, the "free water" content I_{cap} is very similar, almost identical from 2 days to 28 days of hydration, to the white cement paste without silica fume. An increase of the capillary water signal is however observed by ^{1}H NMR at later ages in the presence of silica fume. The reasons for this are not clear and will not be discussed further in this paper but multiple repeats have confirmed this trend.

Concerning T_2 relaxation times (Fig. 1b), the different water populations have very similar magnitudes as for plain white cement. T_2 of the capillary water reservoir rapidly reaches an asymptotic value of 1 ms. The T_2 of the water in gel pores is almost equal for both mixes with a slight decrease with time to circa 320 μs. The T_2 relaxation times of the C–S–H interlayer are however slightly shorter in the case of white cement with silica fume.

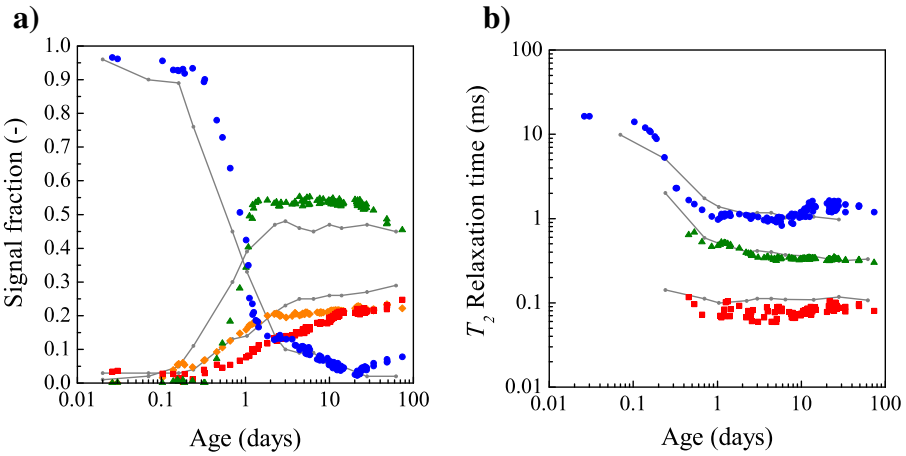

Fig. 1. (a) Evolution of the different water populations as a function of hydration time for white cement with 10% silica fume (colours), all at $w/b = 0.4$. Diamonds are solid signals I_{solid}, squares are C–S–H interlayer water I_{CSH}, triangles are C–S–H gel pore water I_{gel}, and solid circles are "free water" I_{cap}, becoming interhydrate water. The solid signal for the plain white cement mix is not displayed. (b) Evolution of the associated T_2 relaxation times for the different water populations. The grey lines are the equivalent of the mobile fractions and T_2 relaxation times for the plain white cement taken from reference [12].

The T_2 relaxation times could be interpreted according to the fast exchange model [20]. The C–S–H interlayer space has an average T_2 of 80 ± 15 μs, which is smaller than the value reported for plain white cement ($T_2 = 100$ μs, [12]). This lower value could be interpreted as a smaller interlayer space. However, this is difficult to substantiate. The T_2 to pore size interpretation is based upon the fast diffusion model of relaxation which pre-supposes the existence of a surface water layer and bulk pore water. In such a small space, this is clearly of limited application. On-going molecular simulations and calculations of T_1 in nanoscopic planar pores [22–24] suggest that the observed T_2 is very sensitive to the details of surface chemistry in such small pores and may not be solely related to a change in interlayer spaces.

For the gel pore sizes, a very similar trend is observed for both mixes. We calculate an average size of 3.8 nm at 1 day of hydration. This size then goes down progressively to approach an asymptote of 2.5 nm ($T_2 = 320$ μs) after 4 days of hydration. Overall, the addition of 10% of silica fume does not change the characteristic gel pore sizes.

Concerning the capillary water, the initial T_2 value decreases rapidly during the first day of hydration. As for the plain white cement, the capillary pore size plateaus rapidly at about 8 nm with no further decrease. As reported in our earlier publication [12], we believe that this is the size between the growing C–S–H needles. We call those spaces "interhydrate pores". The reservoir of capillary water reaches the interhydrate size at about 1 day of hydration for the silica fume mix. Finally we note that the specimens are sealed so voids and large pores are present but not filled with water. In principle, those voids are the largest pores in the cement pastes.

4.2. Hydration kinetics

Fig. 2a shows the heat flow measured by isothermal calorimetry for white cement paste with 10% of silica fume (solid line) and plain white cement (dashed line), as a function of hydration time. The data are normalised per gramme of cement. There is a clear enhancement of the heat released during the first 10 h of hydration when 10% of the cement is replaced by silica fume. The acceleration period is highly impacted and shows a higher heat flow rate. This reflects the acceleration of the cement reaction at early age due to the important and well-known filler effect of silica fume. This is confirmed by the XRD results in Fig. 3 with $\alpha_c = 0.52$ for the silica fume mix at 1 day compared to $\alpha_c = 0.40$ previously observed for plain white cement [12]. Fig. 2b shows the cumulative heats, H, calculated from the end of the induction period for the

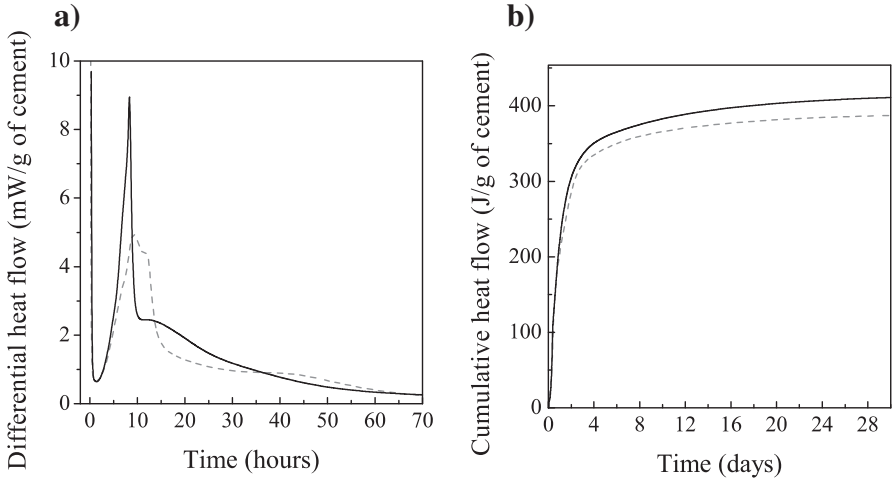

Fig. 2. (a) Heat flows measured during the first 70 h after mixing for white cement with 10% silica fume (solid line) and for plain white cement (dashed line). (b) Cumulative heat flows for the same two mixes.

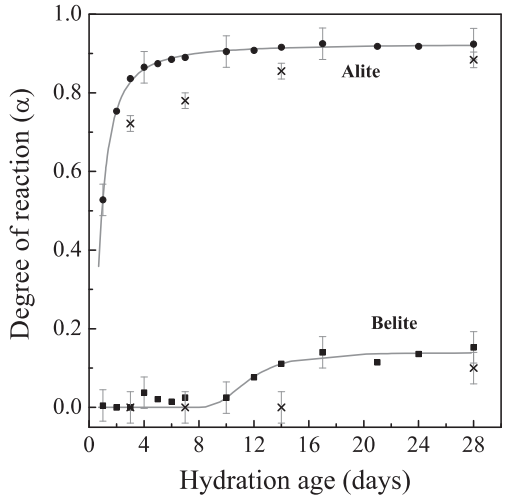

Fig. 3. Degree of reaction of alite (circles) and belite (squares) calculated from XRD and Rietveld quantification and presented as a function of hydration time. The solid grey lines are fits to the data used in the calculation. Crosses are the corresponding values calculated from ^{29}Si MAS NMR. The representative errors are shown for some points only.

same two mixes, expressed in Joules and normalised per gramme of cement. The heat released for white cement with 10% of silica fume becomes significantly higher than plain white cement early in the hydration process.

4.3. Degrees of reaction of alite and belite

Fig. 3 shows the respective degrees of hydration of alite (C_3S) and belite (C_2S) calculated from XRD measurements and Rietveld quantification for the paste which incorporates 10% of silica fume. The XRD data points presented at each age are average values between samples measured as a slice and samples measured after drying as a powder; the measurement error is presented in the figure. According to the XRD patterns, no other cement phases are left unreacted after 1 day of hydration — i.e., C_3A is completely reacted. Fig. 3 reveals that alite reacts mainly during the first 3 days of hydration and reaches $\alpha_{C3S} = 0.84$ at this time. Belite does not show any reaction before 12 days and seems to start dissolving only when the alite reaction has slowed down significantly. At 28 days, $\alpha_{C2S} = 0.15$.

Following previous work in this field [25–28], both C_3S and C_2S trends were fitted using two-component, three-parameter exponential functions (grey lines in Fig. 3)

$$\alpha = \alpha_1 \cdot e^{-\left(\frac{B_1}{t}\right)^{C_1}} + \alpha_2 \cdot e^{-\left(\frac{B_2}{t}\right)^{C_2}} \quad (6)$$

for which the parameters are shown in Table 1.

The two fitted behaviours are used to interpolate between experimental points and are inputs for α_{C3S} and α_{C2S} in Eq. (3).

Table 1
Fitting parameters based on Eq. (6) for the degrees of reaction of alite and belite from XRD; and for the degree of reaction of silica fume from ^{29}Si MAS NMR.

	α_{C3S}	α_{C2S}	α_{sf}
α_1	0.92	0.14	1.85
B_1 (days)	0.67	11.0	27.3
C_1	1.5	6.0	0.26
α_2	2.0	7.1	–
B_2 (days)	87	87	–
C_2	3.0	3.0	–

Table 2
^{29}Si MAS NMR results: degrees of reaction for alite and belite (α_{C3S} and α_{C2S}), C–S–H mean chain length (MCL), chain length of silicate tetrahedra (CL_{Si}) and the Al(IV)/Si ratio of the C–S–H as a function of hydration time.

	α_{C3S}	α_{C2S}	MCL	CL_{Si}	Al/Si
3 days	0.72	0	2.98	2.51	0.055
7 days	0.78	0.00	3.02	2.51	0.059
14 days	0.86	0.00	3.20	2.67	0.059
28 days	0.88	0.10	3.29	2.80	0.052

The overall degree of cement reaction can be calculated as

$$\alpha_c = 1 - [f_{C3S}(1-\alpha_{C3S}) + f_{C2S}(1-\alpha_{C2S})]. \quad (7)$$

The degrees of hydration of alite and belite as calculated from ^{29}Si MAS NMR (see Table 2) are also presented in Fig. 3. While both techniques show similar values at later ages ($\alpha_{C3S} = 0.92 \pm 0.04$ by XRD whereas ^{29}Si MAS NMR gives $\alpha_{C3S} = 0.88 \pm 0.02$ at 28 days of hydration), there is a larger discrepancy for the alite reaction during the first 10 days of hydration. The reasons for this discrepancy are not clear. Poulsen et al. [29] reported that the alite content in anhydrous Portland cements may be overestimated by ^{29}Si NMR in comparison to XRD-Rietveld results due to the presence of Fe^{3+} guest-ions in the alite lattice. Moreover, they stated that the amount of alite may be underestimated in the XRD quantification as a result of small amounts of amorphous phases [29]. Thereby, the variation of alite contents in Fig. 3 highlights the errors associated with the two measurement techniques.

4.4. Silica fume: degree of reaction

^{29}Si MAS NMR experiments were carried out on samples after 3, 7, 14 and 28 days of hydration. The results for the degree of reaction of silica fume are presented in Fig. 4. 34% of the silica fume has reacted by 3 days and up to 67% after 28 days of hydration. These data were used in a fit with one three-parameter exponential component (Fig. 4, grey line) that was subsequently used for α_{sf} in Eqs. (1)–(3). The details of the fit for α_{sf} are reported in Table 1.

Analysis of the ^{29}Si MAS NMR spectra presented in Fig. 5 provides information about the alite and belite degree of reaction based on intensities of deconvoluted spectra. The deconvolutions have been performed using the same approach as described and illustrated recently for hydrated white Portland cements [30] and white Portland cement–metakaolin blends [31]. In comparison with the latter blends, the ^{29}Si MAS NMR spectra of the hydrated white cement–silica fume samples

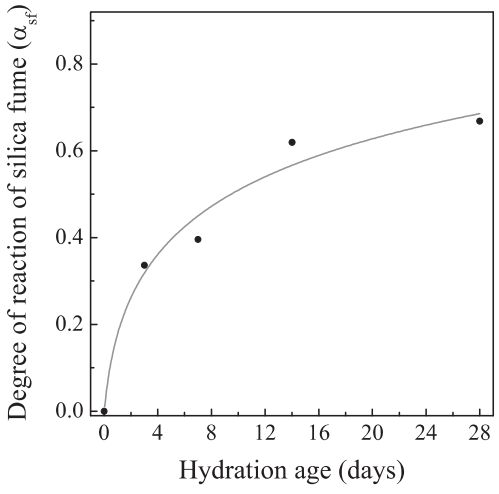

Fig. 4. Degree of reaction for silica fume measured by ^{29}Si MAS NMR. The grey line is a fit to the data (see Table 1).

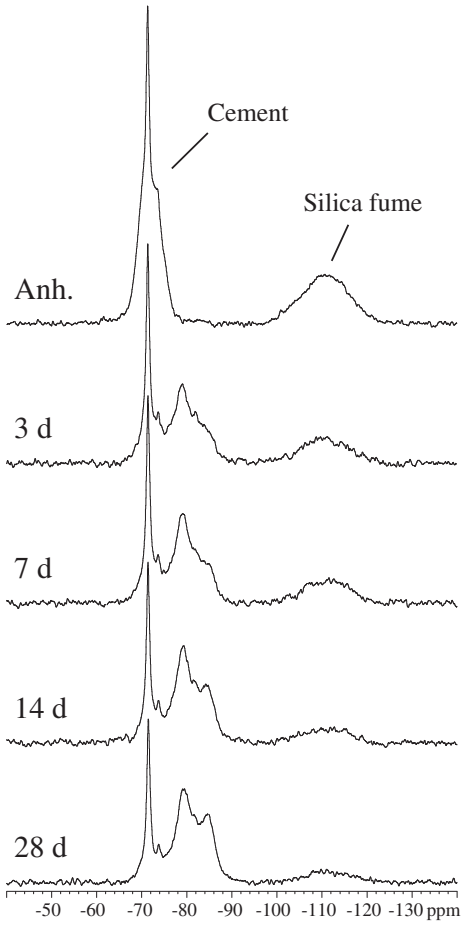

Fig. 5. ^{29}Si MAS NMR spectra (9.4 T, $\nu_R = 6.0$ kHz) of the anhydrous white cement with silica fume and of the blend after hydration for 3, 7, 14 and 28 days.

are easier to analyse since the resonance from silica fume does not overlap with the C–S–H peaks. The results are presented in Table 2 and reported in Fig. 3. Estimated error limits for α_{C3S} and α_{C2S} are ± 0.02 and ± 0.04 respectively. Based on the work of Richardson et al. [32] and Andersen et al. [33], it is possible to calculate from ^{29}Si MAS NMR data the mean aluminosilicate chain length (MCL), the chain length of pure SiO_4 tetrahedra (CL_{Si}) and the Al(IV)/Si ratio of the C–S–H. These data, summarized in Table 2, reveal that both MCL and CL_{Si} increase with the time of hydration, showing that the C–S–H incorporates more Si in its structure. The Al(IV)/Si ratio of the C–S–H is almost invariant with the hydration time, in agreement with earlier ^{29}Si MAS NMR studies of C–S–H phases formed in hydrated white Portland cement [34]. The error limits for MCL and CL_{Si} are ± 0.15 and for Al(IV)/Si it is estimated to ± 0.01.

4.5. Crystalline phases: ettringite and portlandite content

The amount of ettringite for the white cement paste with silica fume, as determined by XRD and Rietveld analysis, is presented as a function of time in Fig. 6. The data are normalised per gramme of cement. Ettringite is formed in the first day and stays constant through the analysis (1–28 days). We do not observe any transformation of ettringite into tricalcium–monosulfo–aluminate hydrate (AFm) as the white cement contains a low amount of C_3A. The average ettringite content is $m_{ett} = 0.089 \pm 0.010$ g/g of cement. The mass fraction of C_3A used for ettringite formation, f_{C3A}^{ett}, per gramme of cement, can then be calculated as $f_{C3A}^{ett} = (m_{ett}/ett^{AMU}) \cdot C_3A^{AMU} = 0.019$ where $ett^{AMU} = 1255$. The rest of the aluminium is assumed to be within the C–S–H through the parameter n_{Al}^{CSH}. The constant value of f_{C3A}^{ett} is used

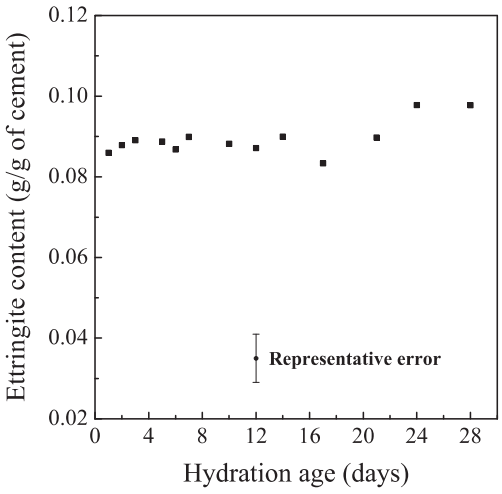

Fig. 6. Mass of ettringite as a function of time, in g/g of anhydrous cement, measured by XRD and Rietveld analysis.

for the calculation in Eq. (3) throughout the hydration. Following the same principle, I_{ett} (the fraction of water in ettringite) can be calculated using $I_{ett} = (0.9 \cdot m_{ett}/ett^{AMU} \cdot H_2O_{ett}^{AMU})/(w/b) = 0.092$, where $H_2O_{ett}^{AMU}$, the atomic mass unit of water in ettringite, is equal to 576.

Assuming $I_{ett} = 0.092$ and that all solid water by ^{1}H NMR comes only from ettringite and portlandite, the mass of portlandite per gramme of cement can be calculated at any time from the ^{1}H NMR data as $m_{CH} = (I_{solid} - I_{ett}) \cdot (w/b) \cdot CH^{AMU}/(H_2O_{CH}^{AMU} \cdot 0.9)$, where $CH^{AMU} = 74$ and $H_2O_{CH}^{AMU} = 18$. The ^{1}H NMR results are presented in Fig. 7, in gramme of portlandite per gramme of cement (filled diamonds), and compared to the results obtained by both XRD (empty squares) and TGA (grey inverted triangles); the relative error bar on the figure indicates the uncertainty. The different techniques are in reasonably good agreement with each other. The jumps in the ^{1}H NMR data are due to the fact that different samples were scanned at different times. Nevertheless, these small shifts stay within the error of the other techniques (around $\pm 1\%$ of the absolute value) and are not considered critical to our analysis.

The portlandite content reaches a plateau after 3 days of hydration with an average value of 0.21 ± 0.01 g/g of cement between both XRD and TGA. For comparison, the grey line in Fig. 7 tracks the behaviour of

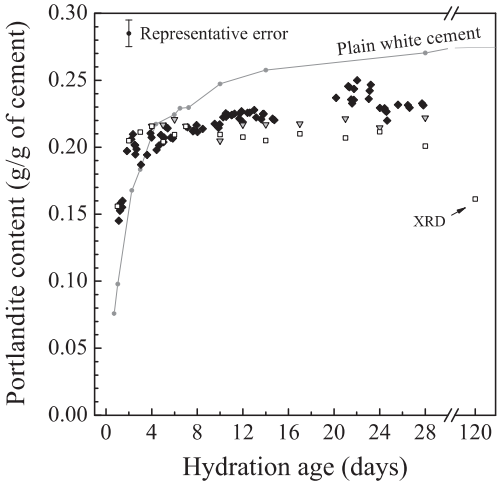

Fig. 7. Mass of portlandite as a function of time, in g/g of anhydrous cement, measured and calculated by ^{1}H NMR (black diamonds), XRD (empty squares) and TGA (grey inverted triangles). The grey line shows the CH content of plain white cement taken from [12].

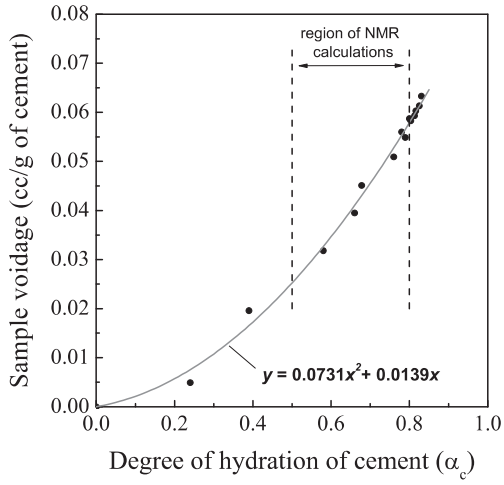

Fig. 8. Chemical shrinkage volume in cm^3/g of cement as a function of cement hydration for the white cement and 10% silica fume mix. The solid line is a polynomial fit to the data. The "region of NMR calculations" illustrates the part of the curve used for the density calculation.

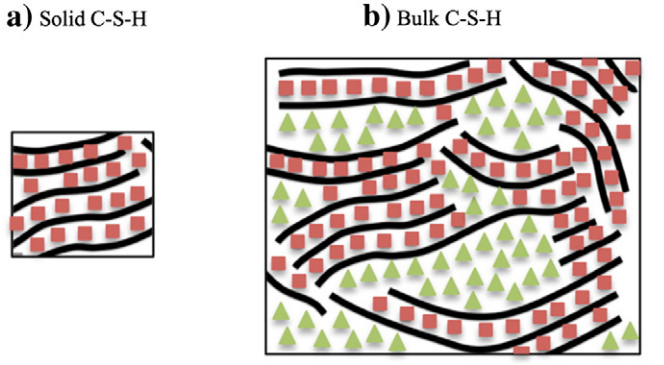

Fig. 9. Graphical representation of the C–S–H as seen by ^1H NMR. The solid lines are the calcium oxide layers with silicate tetrahedra attached on both sides; the red squares are the interlayer water and the green triangles represent the gel water. The figure illustrates what we define as "solid C–S–H" and "bulk C–S–H".

the plain white cement where we see a continuous increase of the portlandite content with time. The faster increase at early age for the silica fume mix is due to the acceleration of the cement hydration by the filler effect of silica fume noted by calorimetry. The apparent consumption of CH by the pozzolanic reaction with silica fume at 28 days of hydration is 0.05 g/g of cement. A further decrease is observed at 120 days when $m_{CH} = 0.16$ g/g of cement measured by XRD. This is a decrease of 25% compared to the 28 days CH content. We note that all measurements were performed on sealed systems with empty pores due to chemical shrinkage so there might be a chemical isolation of the calcium hydroxide. As discussed below it is also seen that the calcium content of the C–S–H is lower in the silica fume system, indicating that this calcium is also available for the pozzolanic reaction.

4.6. Chemical shrinkage

The chemical shrinkage results, in cm^3 per gramme of cement, are presented in Fig. 8 as a function of degree of cement hydration. The evolution of voidage with the degree of hydration of cement is not linear due to the contribution of silica fume to the total chemical shrinkage volume. The data were fitted as shown in the figure using a polynomial function (written in Fig. 8). Only the part between the dashed lines is used for C–S–H density calculation.

4.7. Calculation of the C–S–H parameters

The distinction of water into both interlayer and gel pore spaces of C–S–H allows us to consider separately what we call "solid C–S–H" and "bulk C–S–H" as defined in [12,13]. The "solid C–S–H" includes the Ca–O backbone layers with SiO_2 tetrahedra and the interlayer water in between but excludes the water and any hydroxyls on the outer surface of the stacked layers. The "bulk C–S–H" is the C–S–H inclusive of the gel water. Both solid and bulk C–S–H are illustrated schematically in Fig. 9. The ^1H NMR densities are average densities of all C–S–H formed at the time of measurement.

The data presented above allow us to calculate the C–S–H characteristics according to Eqs. (1)–(5). The calculated C–S–H solid and bulk densities are shown in Fig. 10a; the Ca/(Si + Al) ratio of the C–S–H in Fig. 10b; and the solid and bulk C–S–H water contents in Fig. 10c and d. Taken together these results give a complete description of hydrating white cement paste with 10% of silica fume from 1 day to 28 days. The results are interdependent as all equations are solved together. The data are compared to the plain white cement results from reference [12] (grey lines).

To study the impact of potential errors, extra points in these graphs were calculated using the degrees of alite and belite reaction from ^{29}Si MAS NMR at 3 days and 28 days of hydration (cross symbols). The sensitivity of the results to the measured values is discussed further below. Nevertheless, it is interesting to note this alternate analysis has more impact on some values and little on others.

The average bulk density of the C–S–H increases with time between 1 day and 28 days of hydration. This densification of the average C–S–H material reflects the fact that no more gel pore is created beyond 1 day. Two densification regimes are observed. The end of the first regime of fast densification corresponds to the slowdown of the alite reaction (Fig. 3). The C–S–H bulk density calculated at 28 days, $\rho_{x'} = 1.94 \pm 0.01$ g/cm^3, is close to the values usually reported in the literature [3] and similar to the one we have calculated in [12] for plain white cement paste at the same hydration age: $\rho_{x'} = 1.96$ g/cm^3. In the same way, the solid C–S–H density at 28 days, $\rho_x = 2.75 \pm 0.01$ g/cm^3, is almost the same as the one reported for plain white cement paste, $\rho_x = 2.74$ g/cm^3 [12]. We note a higher solid C–S–H density observed initially at 1 day with $\rho_x = 2.91 \pm 0.01$ g/cm^3 compared to $\rho_x = 2.73$ g/cm^3 for plain white cement. However, this early age difference is difficult to substantiate as early age properties are more difficult to capture experimentally. This discrepancy does not occur for the value calculated when using, at 3 days, the α_{C3S} estimated by ^{29}Si MAS NMR.

For the C–S–H water contents, inclusive x' and exclusive x of the gel water (Fig. 10c), we observe the inverse trends to the densities. The slight increase of x and the decrease of x' with time are a result of densification. The total water content of C–S–H goes down from circa $x' = 5.50$ H_2O/(Si + Al) at 1 day of hydration to $x' = 3.84$ at 28 days. The main differences compared to plain white cement are the absolute water contents. The values normalised per silicon and aluminium moles are significantly lower than without incorporation of silica fume. We report an average solid C–S–H water content of $x = 1.10$ H_2O/(Si + Al) beyond 20 days of hydration. This is a decrease of 39% compared to $x = 1.80$ for plain white cement [12]. However, when the water contents are normalised by calcium in C–S–H (Fig. 10d), the two mixes present much more similar values. Solid C–S–H nonetheless shows slightly lower H_2O/Ca than for the plain white cement.

We calculate an average Ca/(Si + Al) = 1.60 ± 0.04 for the C–S–H produced during the first 2 days of hydration. This is lower than for plain white cement with Ca/(Si + Al) > 1.80 at early age (grey line in

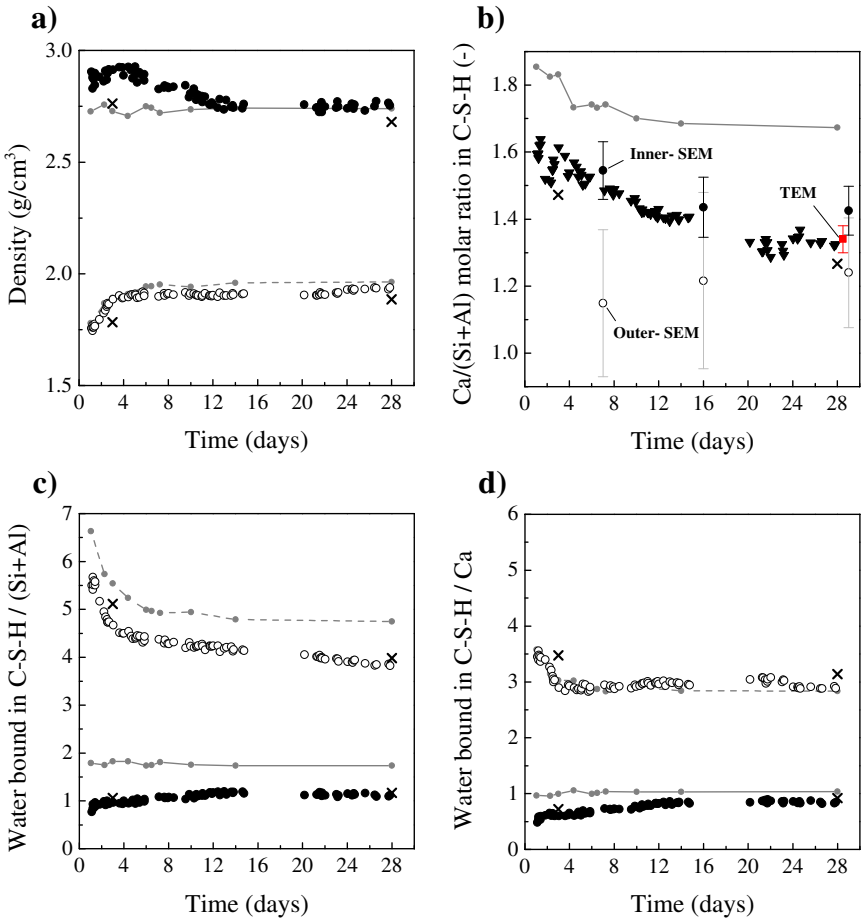

Fig. 10. Calculation results for the white cement paste including 10% silica fume prepared with $w/b = 0.4$ as a function of hydration time. The grey lines in all figures show the behaviour of plain white cement taken from [12]. (a) C–S–H density: solid symbols are C–S–H solid density, exclusive of the gel water; empty symbols are for C–S–H bulk density, inclusive of the gel water. (b) Average Ca/(Si + Al) ratio of the C–S–H calculated from ^{1}H NMR (black inverted triangles); estimated by SEM–EDX for inner-C–S–H (solid circles) and outer-C–S–H (empty circles) and by TEM–EDX (red square). (c) and (d) Associated water contents for the solid and bulk C–S–H. The crosses in all figures show the results when the degree of alite and belite reaction was taken from ^{29}Si MAS NMR instead of XRD at 3 days and 28 days of hydration.

Fig. 10b). This is related to the fact that 15% of the silica fume has already reacted after 2 days (Fig. 4) and that this silicon is incorporated in the C–S–H structure. As the hydration of cement and silica fume proceeds, this average ratio goes progressively down to Ca/(Si + Al) = 1.33 ± 0.04 at 28 days. The calculated Ca/(Si + Al) values are in good agreement with TEM analyses as discussed below.

The complete chemical composition for the bulk C–S–H inclusive of the gel water, at 1 day, is $Ca_{1.60}(Si_{0.94},Al_{0.06})O_{3.57}(H_2O)_{5.50}$. At the other end of the range, the solid C–S–H chemical composition exclusive of the gel water, at 28 days, is $Ca_{1.33}(Si_{0.97},Al_{0.03})O_{3.33}(H_2O)_{1.10}$. This shows that C–S–H is characterised by various compositions dependent on whether the gel water is included and on the hydration

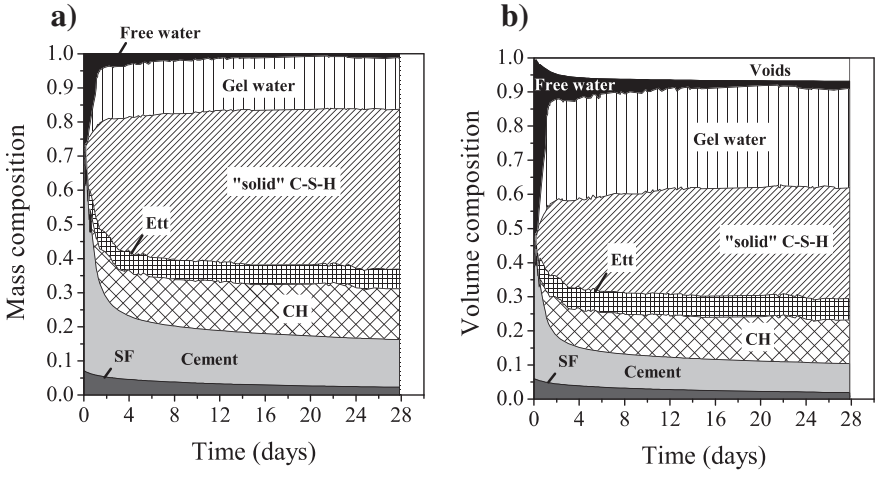

Fig. 11. The mass (a) and volume (b) compositions of the paste as a function of time. The different populations are shown on the graphs.

time at which C–S–H is probed. There is some uncertainty in these values, particularly for the Al/Si ratio. The Al/Si values calculated from the ^{1}H NMR data decrease with time due to the assumption that all the C_3A (only alumina containing component) has reacted at one day whereas in fact the alite and belite phases also contain some alumina in solid solution which is not accounted for and is released later. The Al/Si ratios calculated at early age (0.06 at 1 day) are consistent with the ^{29}Si MAS NMR values (0.052–0.059) reported in Table 2.

Using the C–S–H density and chemical composition as calculated above, the evolution of the mass and volume composition of the paste with silica fume can be drawn, for instance, as a function of hydration time as shown in Fig. 11.

4.8. SEM and TEM microscopy

Our calculation gives substantially lower Ca/(Si + Al) ratios for white cement mixed with 10% of silica fume compared to plain white cement (Fig. 10b). In order to confirm experimentally the decrease in Ca/(Si + Al) ratio of the silica fume blend, SEM–EDX quantifications were carried out at 7, 16 and 29 days of hydration. Using backscattered images and point analysis, outer- and inner-C–S–H can be distinguished [35] and quantified separately. The results for both the inner- and outer-C–S–H Ca/(Si + Al) ratios are reported in Table 3 and compared to the ^{1}H NMR results in Fig. 10b. We note that in the experimental conditions, the interaction volume for the electrons is of the order of cubic micrometres. For this reason, a reliable quantification of outer-C–S–H becomes difficult due to intermixing with fine silica fume particles. Inner-products, localized within the original cement grains, are less sensitive to this effect [36].

The SEM data for the inner-C–S–H show slightly higher Ca/(Si + Al) values than the ^{1}H NMR calculation. However, the ^{1}H NMR values are average chemical compositions and no distinction is possible between inner- and outer-products. A decrease of Ca/(Si + Al) ratio with time is still observed for both ^{1}H NMR and inner-C–S–H by SEM. On the other hand, the estimated Ca/(Si + Al) of outer-C–S–H appears to increase with time. This reflects the artefact of intermixing with unreacted silica fume. As silica fume reacts, the outer-C–S–H quantification approaches the ^{1}H NMR value.

A TEM–EDX quantification of the C–S–H Ca/(Si + Al) was obtained at 28 days on the same mix (red square in Fig. 10b). It is easier to avoid interaction with either cement grains or unreacted silica fume by TEM–EDX analysis as it probes thin sections of C–S–H where the interaction volume is much smaller. The results give Ca/(Si + Al) = 1.34 ± 0.04, which is in between the SEM inner- and outer-quantification and almost identical to the ^{1}H NMR estimate at 28 days.

The second advantage of the TEM is the possibility of seeing C–S–H morphology. Fig. 12 shows a TEM bright field electron image of one of the thin sections under study. It is clear from the image that the C–S–H displays a more fine, foil-like structure than fibrils. Richardson [37] reports that this feature is representative of a Ca/Si < 1.5. This was further confirmed by the recent work of Rossen [38] when studying various blended systems. In our work, the foil-like morphology observed by TEM is then consistent with the Ca/(Si + Al) ratios reported in Table 3 (1.34 ± 0.04 measured by TEM and 1.33 ± 0.04 measured by ^{1}H NMR at 28 days).

Table 3
SEM–EDX and TEM–EDX Ca/(Si + Al) ratios at different hydration ages. The values are compared to the ^{1}H NMR Ca/(Si + Al) estimates.

Age (days)	Outer-CSH by SEM	Inner-CSH by SEM	TEM	Average ^{1}H NMR
7	1.15 ± 0.22	1.54 ± 0.09	–	1.48 ± 0.04
16	1.22 ± 0.26	1.43 ± 0.09	–	1.40 ± 0.04
28/29	1.24 ± 0.16	1.42 ± 0.07	1.34 ± 0.04	1.33 ± 0.04

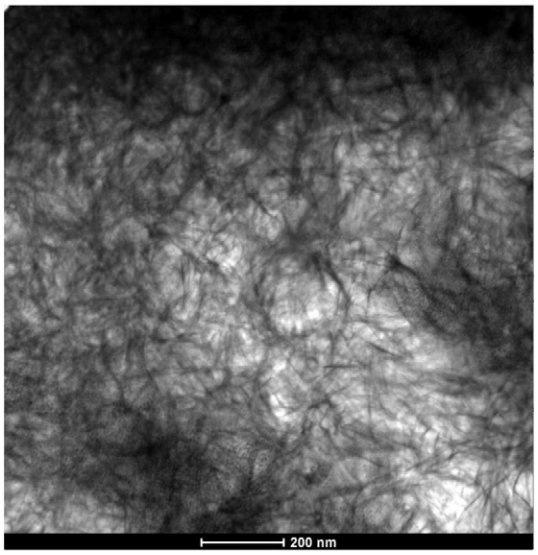

Fig. 12. TEM micrograph of white cement paste with 10% of silica fume at 28 days of hydration. The image displays the foil-like structure of C–S–H.

4.9. Sensitivity analysis

The C–S–H parameters presented above depend on many different measured values through the system of Eqs. (1)–(5). In Table 4 we show the sensitivity of these parameters to variations in the experimental values. While the ettringite and the voidage fraction have little impact on the calculations, a 5% change in the degree of reaction of cement affects all results by 2.5% to 5%. A 5% change in the degree of reaction of silica fume impacts the chemical composition by 1.5%. The total ^{1}H NMR signal is kept constant. A 5% change in the I_{solid} ^{1}H NMR signal compensated by a weighted change of the ^{1}H NMR liquid signals seems to have an important effect on the Ca/(Si + Al) ratio of the C–S–H as portlandite contains a lot of Ca. A 5% decrease of the gel fraction, I_{gel}, with a compensating increase to the benefits of the interlayer signal, I_{CSH}, has the stronger effect and impacts the solid water content of the C–S–H up to 12%.

The difference in the values obtained based on the degree of reaction of alite by XRD and ^{29}Si MAS NMR shown in Fig. 3 highlights the possible discrepancies particularly at early age. Nevertheless at later ages the values seem to be highly self-consistent, in particular with excellent agreement in the C–S–H composition measured by TEM and that calculated from the ^{1}H NMR. This gives us confidence in the absolute values from around 12 days.

Table 4
Sensitivity study of C–S–H density, water content and Ca/(Si + Al) calculation at 28 days of hydration.

Parameter changed by −5%	Solid C–S–H density	Solid H_2O/Si	Ca/(Si + Al)	Bulk C–S–H density
Initial values	2.75	1.10	1.25	1.93
Ettringite (g/g of cement)	−0.06%	−0.32%	−1.55%	−0.14%
DOH cement (α_c)	−2.65%	4.94%	−3.05%	−2.64%
DOH SF (α_{sf})	0.11%	1.45%	1.55%	−0.06%
Voidage (cm^3/g of cement)	−1.06%	0.00%	−0.01%	−0.57%
NMR I_{solid} (with change in I_{liquid})	0.15%	1.69%	4.48%	0.44%
NMR I_{gel} (with change in I_{CSH})	−2.69%	12.14%	0.13%	0.00%

5. Discussion and conclusion

This study has confirmed the impact of silica fume on hydration kinetics. There is an enhancement of the cement reaction at early age due to the small size and high surface area of the silica fume which increases the C–S–H nucleation. However, the evolution of the different water populations follows a very similar pattern in the system with silica fume to those without, indicating no fundamental change in the underlying mechanisms.

Several phenomena occur simultaneously at 1 day. In addition to the plateau of the gel pore water intensity, there is an important change in the rate of consumption of capillary water. This moment coincides with the time at which the capillary pore size reaches 8 nm, the interhydrate specific size. This behaviour, observed previously for the plain white cement [12], suggests at this stage that the hydration processes in cement paste are affected by the lack of water filled space for C–S–H growth.

The changes in the C–S–H due to the pozzolanic reaction also confirm previous findings of a decrease in the Ca/(Si + Al) ratio of the C–S–H. Based on the C–S–H analogue structure of tobermorite, part of this decrease may be the addition of some silicon bridging tetrahedra in between silicon dimers: the ^{29}Si MAS NMR data reported in Table 2 shows a slight rise of the average chain length of SiO_4 tetrahedra (CL_{Si}) from 2.51 to 2.80. Therefore the main change is probably less calcium ions in the interlayer.

The results of this study show a significant decrease of the Ca/Si ratio of the C–S–H while the consumption of portlandite is rather small (Fig. 7). A simple calculation based on the amount of silica fume reacted and the resulting C–S–H composition indicates that only about a quarter of the calcium needed to form C–S–H from the silica fume comes from portlandite, the rest of the calcium comes from the C–S–H formed in the early stages of reaction from the reaction of alite (before silica fume is much reacting).

The analysis of ^{1}H NMR signals allows us to take the analysis further by quantifying the different water populations and calculating C–S–H characteristics. It indicates a growth of C–S–H similar to that observed for plain white cement where gel pores stop forming within the first days. Densities and the overall water content of the C–S–H are very similar at 28 days and no major structural difference is observed. Pore sizes between plain white cement and white cement with silica fume are also very similar.

Acknowledgement

We thank Y.-Q. Song of Schlumberger-Doll Research for 2D Fast Laplace Inversion software. The white Portland cement was provided by Aalborg Portland A/S, Cementia Holding ApS, Denmark. The research leading to these results has received funding from the European Union Seventh Framework Programme (FP7/2007–2013) under grant agreement 264448. JS acknowledges the Danish Strategic Research Council (No.11-116724) for financial support to the LowE-CEM project. PJM thanks the Nanocem (www.nanocem.org) and the UK Engineering and Physical Sciences Research Council (grant number: EP/H033343/1) for their financial support. We thank John Rossen from LMC, EPFL for the TEM measurements. We thank Sika Technology Centre in Zurich for the measurement of silica fume density.

References

[1] H.E. Petch, The hydrogen positions in portlandite, $Ca(OH)_2$, as indicated by the electron distribution, Acta Crystallogr. 14 (9) (1961) 950–957.
[2] L. Desgranges, D. Grebille, G. Calvarin, G. Chevrier, N. Floquet, J.C. Niepce, Hydrogen thermal motion in calcium hydroxide: $Ca(OH)_2$, Acta Crystallogr. Sect. B: Struct. Sci. 49 (5) (1993) 812–817.
[3] H. Jennings, Refinements to colloidal model of C–S–H in cement: CM-II, Cem. Concr. Res. 38 (2008) 275–289.
[4] C. Famy, K.L. Scrivener, A. Atkinson, Effects of an early or a late heat treatment on the microstructure and composition of inner C–S–H products of Portland cement mortars, Cem. Concr. Res. 32 (2) (2002) 269–278.
[5] A. Nonat, The structure and stoichiometry of C–S–H, Cem. Concr. Res. 34 (2004) 1521–1528.
[6] E. Gallucci, X. Zhang, K.L. Scrivener, Effect of temperature on the microstructure of calcium silicate hydrate (C–S–H), Cem. Concr. Res. 53 (2013) 185–195.
[7] W. Gutteridge, J. Dalziel, Filler cement. The effect of the secondary component on the hydration of portland cement: part 1. A fine non-hydraulic filler, Cem. Concr. Res. 20 (1990) 778–782.
[8] J. Skibsted, O.M. Jensen, H.J. Jakobsen, Hydration kinetics for the alite, belite, and calcium aluminate phase in Portland cements from ^{27}Al and ^{29}Si MAS NMR spectroscopy, 10th International Congress on the Chemistry of Cement, Göteborg 1997, p. 2ii056.
[9] H. Justnes, I. Meland, J.O. Bjoergum, J.A. Krane, ^{29}Si MAS NMR study of the pozzolanic activity of condensed silica fume and the hydration of di- and tricalcium silicates, Adv. Cem. Res. 3 (1990) 111–116.
[10] H. Justnes, E.J. Sellevold, G. Lundevall, High strength concrete binders. Part A: reactivity and composition of cement pastes with and without condensed silica fume, 4th International Conference on Fly Ash, Silica Fume, Slag and Natural Pozzolans in Concrete, Istanbul 1992, pp. 873–889.
[11] A. Valori, P.J. McDonald, K.L. Scrivener, The morphology of C–S–H: lessons from ^{1}H nuclear magnetic resonance relaxometry, Cem. Concr. Res. 49 (2013) 65–81.
[12] A.C.A. Muller, K.L. Scrivener, A.M. Gajewicz, P.J. McDonald, Densification of C–S–H measured by ^{1}H NMR relaxometry, J. Phys. Chem. C 117 (2013) 403–412.
[13] A.C.A. Muller, K.L. Scrivener, A.M. Gajewicz, P.J. McDonald, Use of bench-top NMR to measure the density, composition and desorption isotherm of C–S–H in cement paste, Microporous Mesoporous Mater. 178 (2013) 99–103.
[14] T.C. Powers, T.L. Brownyard, Studies of the Physical Properties of Hardened Portland Cement Paste; Portland Cement Association (Bulletin 22): Chicago, 1948. (reprinted from Proc. J. Am. Concr. Inst. 1947, 43, p. 101, 249, 469, 549, 669, 845, 993).
[15] J.G. Powles, J.H. Strange, Zero time resolution nuclear magnetic resonance transients in solids, Proc. Phys. Soc. Lond. 82 (1963) 6–15.
[16] S. Meiboom, D. Gill, Modified spin-echo method for measuring nuclear relaxation times, Rev. Sci. Instrum. 29 (1958) 688–691.
[17] L. Venkataramanan, Y.Q. Song, M.D. Hürlimann, IEEE Trans. Signal Process. 50 (2002) 1017–1026.
[18] P.J. McDonald, V. Rodin, A. Valori, Characterisation of intra- and inter-C S H gel pore water in white cement based on an analysis of NMR signal amplitudes as a function of water content, Cem. Concr. Res. 40 (2010) 1656–1663.
[19] K.R. Brownstein, C.E. Tarr, Importance of classical diffusion in nmr studies of water in biological cells, Phys. Rev. A 19 (6) (1979) 2446–2453.
[20] F. D'Orazio, S. Bhattacharja, W.P. Halperin, K. Eguchi, T. Mizusaki, Phys. Rev. B42 (1990) 9810–9818.
[21] W.P. Halperin, J.Y. Jehng, Y.Q. Song, Application of spin–spin relaxation to measurement of surface area and pore size distributions in a hydrating cement paste, Magn. Reson. Imaging 12 (1994) 169–173.
[22] D.A. Faux, P.J. McDonald, N.C. Howlett, J.S. Bhatt, S.V. Churakov, Nuclear magnetic resonance relaxometry of water in two and quasi-two dimensions, Phys. Rev. E Stat. Nonlinear Soft Matter Phys. 87 (6) (2013).
[23] J.S. Bhatt, P.J. McDonald, D. Faux, N.C. Howlett, S.V. Churakov, NMR relaxation parameters from molecular simulations of hydrated inorganic nanopores, Int. J. Quantum Chem. (2014).
[24] S.H.P. Cachia, Private Communication.
[25] P. Freiesleben Hansen, J. Pedersen, Maturity Computer for Controlled Curing and Hardening of Concrete, 1, Nord. Betong, 1977. 19–34.
[26] I. Pane, W. Hansen, Investigation of blended cement hydration by isothermal calorimetry and thermal analysis, Cem. Concr. Res. 35 (2005) 1155–1164.
[27] J. Zhang, D. Cusson, L. Mitchell, T. Hoogeveen, J. Margeson, The maturity approach for predicting different properties of high-performance concrete, 7th International Symposium on Utilization of High-Strength/High-Performance Concrete, Washington, ACI SP 228-11, 1 2005, pp. 135–154.
[28] H.K. Kamyab, A.C.A. Muller, E. Denarié, K.L. Scrivener, E. Brühwiler, Kinetics of water repartition in UHPFRC using ^{1}H NMR, Cem. Concr. Res. (2015) (in preparation).
[29] S.L. Poulsen, V. Kocaba, G. Le Saoût, H.J. Jakobsen, K.L. Scrivener, J. Skibsted, Improved quantification of alite and belite in anhydrous Portland cements by ^{29}Si MAS NMR: effects of paramagnetic ions, Solid State Nucl. Magn. Reson. 36 (2009) 32–44.
[30] J. Skibsted, M.D. Andersen, The effect of alkali ions on the incorporation of aluminum in the calcium silicate hydrate (C–S–H) phase resulting from Portland cement hydration studied by ^{29}Si MAS NMR, J. Am. Ceram. Soc. (2013) 651–656.
[31] Z. Dai, T.T. Tran, J. Skibsted, Aluminum Incorporation in the C–S–H phase of white Portland cement–metakaolin blends studied by ^{27}Al and ^{29}Si MAS NMR spectroscopy, J. Am. Ceram. Soc. 97 (2014) 2662–2671.
[32] I.G. Richardson, The characterization of hardened alkali-activated blast-furnace slag pastes and the nature of the calcium silicate hydrate (C–S–H) phase, Cem. Concr. Res. 24 (5) (1994) 813–829.
[33] M.D. Andersen, H.J. Jakobsen, J. Skibsted, Characterization of white Portland cement hydration and the C–S–H structure in the presence of sodium aluminate by ^{27}Al and ^{29}Si MAS NMR spectroscopy, Cem. Concr. Res. 34 (2004) 857–868.
[34] M.D. Andersen, H.J. Jakobsen, J. Skibsted, Incorporation of aluminum in the calcium silicate hydrate (C–S–H) of hydrated Portland cements: a high-field ^{27}Al and ^{29}Si MAS NMR investigation, Inorg. Chem. 24 (2003) 2280–2287.
[35] K.L. Scrivener, Microstructure of concrete, in: J. Skalny (Ed.), Materials Science of Concrete, vol. I, American Ceramic Society, Westerville, Ohio 1989, pp. 127–161.
[36] J.E. Rossen, K.L. Scrivener, Optimization of SEM–EDX to determine C–S–H composition in matured cement paste samples, Mater. Charact. J. (2015) (in preparation).
[37] I.G. Richardson, The nature of C–S–H in hardened cements, Cem. Concr. Res. 29 (1999) 1131–1177.
[38] J.E. Rossen, Stability of C–A–S–H in Pastes of Alite and Cement Blended With Supplementary Cementitious MaterialsPhD thesis EPFL, Switzerland 2014.